Simulated decadal variability of the meridional overturning circulation across the A25-Ovide section

Damien Desbruyères,[1] Virginie Thierry,[2] and Herlé Mercier[1]

[1]   Decadal changes of the meridional overturning circulation (MOC) at the A25-Ovide section between Portugal and Greenland are investigated in a numerical simulation forced by atmospheric reanalysis data for the period 1965–2004. The intensity, composition, and structure of the upper MOC limb are assessed using a Lagrangian analysis tool. Its mean transport is fed by water masses of two distinct origins: the subtropics and the Labrador Sea. Two vertical overturning cells are consequently identified: a subtropical cell connecting low and high latitudes (12 Sv, $1 \, \text{Sv} = 10^6 \, \text{m}^3 \, \text{s}^{-1}$) and a cell internal to the subpolar gyre (4 Sv). The decadal MOC variability is associated with synchronized transport changes of the subtropical and subpolar inflow within the North Atlantic Current (NAC). The varying strength of the MOC is further related to changes in the upper horizontal transport distribution. When the MOC is in a strong phase (early 1990s), the northern branch of the NAC in the Iceland Basin is strong while the southern branch at the Rockall Trough entrance is relatively weak. The inverse situation holds for a persistent weak MOC state (1970s). Contrary to the conclusions of earlier studies, variability in the strength and shape of the subpolar gyre does not stand as the main driver of the changing NAC structure, which is largely induced by the horizontal variability of the subtropical inflow. Additionally, the recently shown intrusion of subtropical waters into the northeastern Atlantic (late 1960s, early 1980s, and 2000s) are shown to primarily occur during periods of weak MOC circulation at A25-Ovide.

Citation: Desbruyères, D., V. Thierry, and H. Mercier (2013), Simulated decadal variability of the meridional overturning circulation across the A25-Ovide section, *J. Geophys. Res. Oceans*, *118*, 462–475, doi:10.1029/2012JC008342.

1. Introduction

[2]   The quantification and understanding of long-term changes in the redistribution of heat between low and high latitude regions stand as a major challenge in climate research. In the North Atlantic Ocean, this meridional heat transport is mainly carried out by the meridional overturning circulation (MOC)—a vertical circulation cell depicting a northward transport of light waters within its upper limb and a return flow of relatively dense waters at depth. The present study focuses on the MOC variability at the A25-Ovide section joining Cape Farewell (Greenland) and Portugal, and particularly emphasizes decadal changes in the strength, composition, and structure of the warm water transport carried out by the North Atlantic Current (NAC).

[3]   From a dynamical point of view, two prominent and permanent pathways of the NAC east of the Mid-Atlantic Ridge (MAR) are usually described in the literature: a northern

branch, often referred to as the subpolar front, which flows from the Charlie Gibbs Fracture Zone into the Iceland basin as part of the cyclonic subpolar gyre circulation, and a southern branch that flows within the Rockall Trough and that preferentially crosses the Iceland-Scotland Ridge to feed the Nordic Seas [*Bower et al.*, 2002; *Brambilla and Talley*, 2006; *Bower and von Appen*, 2007]. A significant fraction of those surface waters is progressively transformed through air-sea interactions into intermediate and deep water masses during their cyclonic journey around the Iceland and Irminger basins [*Brambilla and Talley*, 2008; *Brambilla et al.*, 2008], and eventually meets the denser overflow waters along the Greenland continental slope to form the deep limb of the MOC [*Lherminier et al.*, 2010; *Sarafanov et al.*, 2012]. Variability in the overflow intensity was found to be relatively small on decadal timescales [*Nilsen et al.*, 2003; *Olsen et al.*, 2008], suggesting that the MOC variability on such timescales reflects the varying rate of light-to-dense water mass conversion south of the Greenland-Iceland-Scotland (GIS) sills.

[4]   Observational evidence of interannual to decadal changes in the strength and structure of the MOC in the northeastern subpolar Atlantic Ocean is mainly provided by the analysis of hydrographic sections. The Ovide project was particularly aimed to describe the circulation and the water masses in the eastern subpolar gyre, through the analysis of repeat hydrographic surveys between Portugal and Greenland in the 2000s (the A25-Ovide line, see Figure 1) [*Lherminier et al.*, 2007; *Lherminier et al.*, 2010; *Daniault*

[1]CNRS, Laboratoire de Physique des Océans, UMR6523, IFREMER, CNRS, UBO, IRD, Plouzané, France.
[2]IFREMER, Laboratoire de Physique des Océans, UMR6523, IFREMER, CNRS, UBO, IRD, Plouzané, France.

Corresponding author: D. Desbruyères, CNRS, Laboratoire de Physique des Océans, UMR6523, IFREMER, CNRS, UBO, IRD, Plouzané, France. (damien.desbruyeres@ifremer.fr)
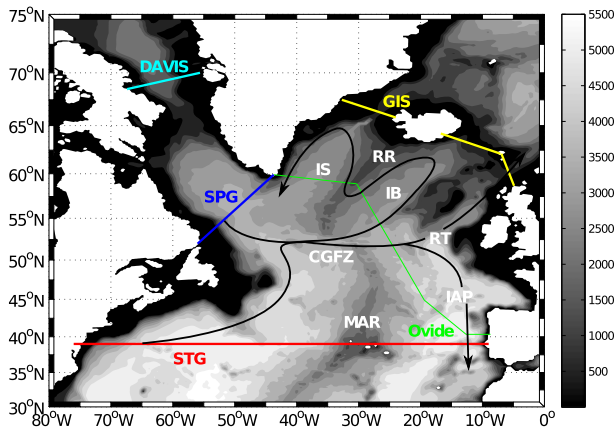
Figure 1. Bathymetry of the northern North Atlantic (in meters) and positions of the sections discussed in the text: the A25-Ovide section (green), the STG transect (red), the SPG transect (blue), the Davis Strait section (cyan), and the GIS section (yellow). The main basins and topographic features mentioned in the text are labeled as: IS (Irminger Sea), IB (Iceland Basin), RT (Rockall Trough), IAP (Iberian Abyssal Plain), MAR (Mid-Atlantic Ridge), CGFZ (Charlie Gibbs Fracture Zone), RR (Reykjanes Ridge). The black lines stand for a simplified view of the main pathways of the North Atlantic Current.

et al., 2011a, 2011b; *Gourcuff et al.*, 2011]. Similar investigations were also carried out at 60°N during the 2000s [*Sarafanov et al.*, 2012] and across the A1E section between Greenland and Ireland during the 1990s [*Bersh*, 2002]. Yet, while those efforts have largely contributed to the current understanding of the MOC structure in this particular region, investigating the decadal oceanic variability from such spatially and temporally sparse measurements is difficult.

[5] The knowledge of global air-sea fluxes of heat, freshwater, and momentum over the last decades has enabled the MOC variability to be addressed through Ocean General Circulation Models (OGCMs) experiments. Those tools have provided crucial information about the North Atlantic MOC and heat transport variability, particularly with regards to its spatial coherence [e.g., *Marsh et al.*, 2005; *Bingham et al.*, 2007; *Böning et al.*, 2006; *Zhang*, 2010] and its response to idealized or observed atmospheric conditions. This response was particularly linked to the dominant mode of atmospheric variability known as the North Atlantic Oscillation (NAO) [*Hurrell*, 1995], which exerts a strong influence on the spatio-temporal distribution of buoyancy and mechanical fluxes at the air-sea interface [e.g., *Häkkinen*, 1999; *Eden and Willebrand*, 2001; *Eden and Jung*, 2001; *Gulev et al.*, 2003; *Böning et al.*, 2006; *Deshayes and Frankignoul*, 2008; *Biastoch et al.*, 2008]. Yet, relatively few studies focused on the local MOC variability in the eastern subpolar gyre. *Marsh et al.* [2005] briefly analyzed the MOC and heat transport variability at A25 in an eddy-permitting model, and related it to similar analysis performed at two other hydrographic sections (AR7W and A5-RAPID). *Treguier et al.* [2006] focused on the MOC variability across the A25-Ovide line in the $\frac{1}{6}°$ Clipper model. The link between the MOC and the large-scale gyre circulation on relatively long timescales is however still missing.

[6] The upper MOC limb in the eastern subpolar gyre is primarily composed of subtropical waters from the Gulf Stream, but is also linked to the cyclonic subpolar gyre circulation through the eastward extension of the Labrador Current that joins the NAC past Newfoundland [e.g., *Rossby*, 1996; *Bower et al.*, 2002; *Reverdin et al.*, 2003]. *Schmitz and McCartney* [1993] showed, from a wide range of observations, a NAC of 20 Sv that includes a 7 Sv $(1 \, \text{Sv} = 10^6 \, \text{m}^3 \, \text{s}^{-1})$ component from the Labrador Sea. In a high-resolution model of the North Atlantic, *Böning et al.* [1996] partitioned the NAC transport within the upper 1000 m depth into a subtropical (14.1 Sv) and a subpolar (7.8 Sv) contribution. The respective signatures of both gyres on the decadal NAC variability were first addressed by *Hátún et al.* [2005]. Using a salinity criterion to extract the respective inflow of subtropical and subpolar waters in the NAC, they found opposite decadal changes in the volume transport of both source waters. Those changes were correlated with the buoyancy-driven intensity of the subpolar gyre, as depicted in the so-called "gyre index" [*Häkkinen and Rhines*, 2004]. The weakening and westward retreat of the subpolar gyre and the subsequent increased transport of subtropical waters toward the Nordic Seas was particularly invoked to explain the sharp warming and salinization of the eastern subpolar gyre in the late 1990s and early 2000s [*Bersh et al.*, 2007; *Holliday*, 2003; *Thierry et al.*, 2008; *Robson*, 2010; *Häkkinen et al.*, 2011; *Yeager et al.*, 2012]. A causal relationship between the subpolar gyre dynamics and hydrographic changes in the northeastern Atlantic was recently dismissed by *Herbaut and Houssais* [2009]. The authors rather proposed the setup of a NAO-related wind-driven anomalous circulation in the intergyre region as a potential driving mechanism [*Marshall et al.*, 2001; *Eden and Willebrand*, 2001]. In addition, *Häkkinen et al.* [2011] recently showed episodes of increased penetration of Gulf Stream waters toward the eastern subpolar gyre (late 1960s, around 1980, and early 2000s), presumably driven by wind-stress variability. The link with the MOC variability in middle-to high-latitude regions remains obscure though.

[7] The present study aims to investigate the spatio-temporal variability of the upper MOC limb across the A25-Ovide section for the period 1965–2004. We will combine a global eddy-permitting simulation with a Lagrangian analysis tool to address the following points: (a) provide a description of the mean structure and composition of the upper MOC limb in the eastern subpolar gyre (ESPG) and relate its decadal variability to subpolar and subtropical transport changes, (b) investigate associated changes in the horizontal structure of the NAC, and (c) examine the link between the MOC variability and the spatial extent of subtropical water masses in the ESPG. The ESPG refers hereafter to the region bounded by the A25-Ovide section and the Greenland-Scotland sills (and hence encompasses part of the intergyre region). The study domain and the different sections discussed in the text are shown in Figure 1. The tools and methods are presented in section 2. Section 3 describes the mean (1965–2004) structure and composition of the upper MOC limb across A25-Ovide. Its decadal variability is assessed in sections 4 and 5, and the link with the NAO is briefly discussed in section 6. Section 7 summarizes the results.

2. Numerical Tools

2.1. The Ocean Model

2.1.1. General Configuration

[8] The study utilizes the ORCA025-G70 simulation from the global configuration ORCA025 of the Nucleus for European Modeling of the Ocean [*Madec*, 2008] coupled with the Louvain-la-Neuve Ice model version 2 [*Fichefet and Maqueda*, 1999]. The ORCA025 numerical characteristics are fully detailed in *Barnier et al.* [2006]. The domain is global and is configured using a tripolar grid with 1442×1021 grid points and a horizontal resolution that increases with latitude (from 27.75 km at equator to 13.8 km at 60°N). The vertical grid consists of 46 z-levels with vertical spacing that increases with depth (6 m near the surface, 250 m at the bottom). The ORCA025 parameterizations comprise a Laplacian mixing of temperature and salinity along isopycnals, a horizontal biharmonic viscosity, and a turbulence closure scheme for vertical mixing.

[9] A complete description of the ORCA025-G70 simulation is provided by *Molines et al.* [2006] and *Treguier et al.* [2007]. It was initialized with the Polar Science Center Hydrographic T/S Climatology [*Steele et al.*, 2001], which consists of the Levitus 1998 climatology [*Levitus et al.*, 1998] everywhere except in the Arctic domain where a blend of the Arctic Ocean Atlas and additional data from the Bedford Institute of Oceanography was added to produce a more realistic Arctic hydrography. The simulation was run from 1958 to 2004 with no spin-up. The forcing data set (referenced as DFS3 by *Brodeau et al.* [2009]) was built using data from various origins at different frequencies. Air temperature, wind, and air humidity data originate from the European Centre for Medium-Range Weather Forecast ERA40 reanalysis for the period 1958–2001 and from the European Centre for Medium-Range Weather Forecast analysis for the period 2002–2004. Daily radiative flux and monthly precipitation fields came from the Coordinated Ocean-ice Experiment [*Griffies et al.*, 2009] database and turbulent fluxes (wind stress, latent, and sensible heat fluxes) were calculated from the Coordinated Ocean-ice Experiment bulk formulae [*Large and Yeager*, 2004]. To minimize the model drift, a global surface salinity restoring (300 days over 50 m) to the Polar Science Center Hydrographic T/S Climatology was incorporated. A surface salinity restoring under the ice cover was maintained with a five-time enhanced coefficient (60 days over 50 m). An additional restoring was also applied at the exit of the Red Sea (60 days over 50 m) and the Mediterranean Sea (100 days over 50 m) for a better representation of the overflows. *Rattan et al.* [2010] showed a strong drift in the freshwater content of the Labrador Sea during the first decade of integration in ORCA025-G70. For our present purpose, we believe the degree of equilibrium achieved by the late 1960s is adequate and that the subsequent signal presumably relates to the prescribed interannual forcing. Additionally, *Huck et al.* [2008] reconstructed a MOC signal in the subpolar North Atlantic from hydrographic data for the period 1955–1998 and showed a close correspondence with the ORCA025-G70 variability. We verified that a twin simulation without any restoring to the surface salinity climatology (ORCA025-KNMI01) yields a very similar North Atlantic MOC signal. The tendencies in our transport time series were therefore

not removed. All the results presented are obtained with monthly model outputs and all time series presented thereafter are annual averages of the monthly time series. Although this relatively low temporal sampling could underestimate the influence of eddies, the use of 5 day model outputs yields similar results when considering the MOC variability. Accordingly, *Treguier et al.* [2006] showed in the Clipper ATL6 model ($\frac{1}{6}^{\circ}$ resolution) a small impact of eddy fluxes on the overturning variability at A25-Ovide.

2.1.2. A First Model Evaluation: the Gyre Index

[10] The model evaluation will be carried out throughout the paper. We will see that the ORCA025-G70 simulation reproduces the main characteristics of the circulation in ESPG, as already demonstrated in *de Boisséson et al.* [2012]. A first glimpse of the model ability to simulate the large-scale variability of the North Atlantic Ocean is provided by the first empirical orthogonal function of the sea-surface height and its associated principal component (Figures 2a and 2b, respectively), referred to as the "gyre index" in the literature [e.g., *Häkkinen and Rhines*, 2004;
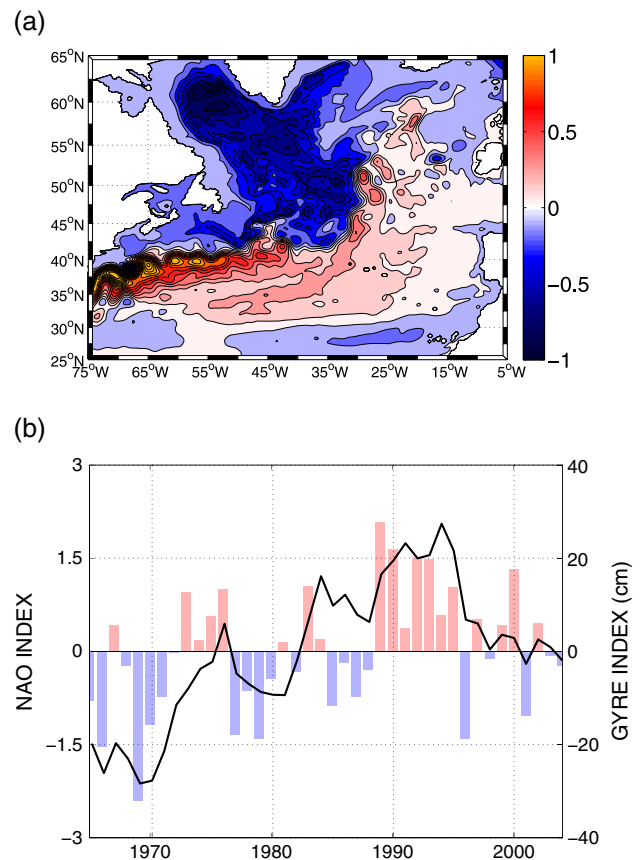
Figure 2. (a) Spatial structure of the first empirical orthogonal function of the simulated sea surface height in ORCA025-G70 (unitless), explaining 18% of the total variance. (b) The associated principal component (in centimeters) with positive anomalies referring to a stronger subpolar gyre circulation and an anticyclonic intergyre gyre. The normalized winter NAO index, defined from the first principal component of the winter sea-level pressure is shown with bars (red: positive NAO years; blue: negative NAO years).

Hátún et al., 2005]. The horizontal structure of the first mode, which explains 18% of the total variance in ORCA025-G70, bears strong resemblance with that obtained from altimetry measurements and shows a clear tripole pattern between the subpolar gyre, the Gulf Stream/intergyre region and low latitudes [*Esselborn and Eden*, 2001; *Häkkinen and Rhines*, 2004]. Note however that the structure of this mode in ORCA025-G70 is more zonal than the one found in observations, possibly due to the southerly path of the NAC between Newfoundland and the MAR in eddy-permitting simulations [e.g., *Böning et al.*, 1996]. Here a positive anomaly in the gyre index refers to a stronger subpolar gyre circulation and an anomalous anticyclonic circulation to the south (the so-called intergyre gyre). The phase and amplitude of the gyre index in ORCA025-G70 is consistent with the observational index of *Häkkinen and Rhines* [2004] and similarly shows the weakening subpolar gyre and the anomalous cyclonic circulation in the Gulf Stream/intergyre region since the mid-1990s (Figure 2b). On longer timescales, the ORCA025-G70 reproduces earlier modeling results with the 1990s gyre index decline preceded by an increasing trend from the mid-1960s to the mid-1990s [*Hátún et al.*, 2005; *Böning et al.*, 2006]. The gyre index variability appears closely related with the fluctuations of the NAO index (correlation of 0.55, significant at the 95% level, not shown), which was also shown in *Häkkinen and Rhines* [2004]. Note that all the correlations given in the following sections (symbolized by *r* hereafter) are calculated for detrended annual time series and are significant at the 95% level.

2.2. The Lagrangian Analysis Tool: ARIANE

[11] The Lagrangian analysis tool ARIANE was extensively used in this study. Its algorithm, based on an off-line volume-preserving scheme, is described in *Blanke and Raynaud* [1997] and *Blanke et al.* [1999]. Its main purpose is to calculate trajectories of numerical particles within a three-dimensional and time-dependent velocity field of an OGCM. For such calculation, the velocity field is assumed to be constant over successive periods equal to the available sampling (monthly averaged velocity field of the ORCA025-G70 simulation will be used). The resulting trajectories are interpreted as the pathways followed by small volume-conservative water parcels advected within the model velocity field from a given initial section to several final sections.

[12] The particles are distributed along the initial section according to the archived Eulerian velocity field at each time step: particles are more numerous in regions where the incoming transport is the largest. In addition, the number of particles within each velocity grid cell was calculated in the present study so that the individual transport attributed to each particle does not exceed 0.5 mSv (we checked that the use of a smaller value, for improved accuracy, leads to very similar results). The sum of all particle transports in each grid cell amounts to the corresponding incoming Eulerian transport. Here the accuracy in the computation of the volume transfer between the initial and final sections is estimated to be 0.1 Sv. Along their paths, particles will change their hydrographic properties according to the local Eulerian fields of the ocean model. Between two successive positions, the temperature and salinity of each particle therefore evolve according to the parameterized thermodynamics

of the model. Supplementary information about ARIANE can be found at http://stockage.univ-brest.fr/grima/Ariane/.

3. The Mean MOC$_\sigma$ Across the A25-Ovide Section: Spatial Structure and Composition

[13] We here focus on the mean structure of the MOC at A25-Ovide. An Eulerian description of the vertical and horizontal shape of both MOC limbs is presented first and compared with available observational estimates. Lagrangian experiments are then used to detail the mean composition of the upper MOC limb.

3.1. The Eulerian View

[14] The A25-Ovide hydrographic section was occupied during summer every other year between 2002 and 2010, and the subsequent analysis of the circulation represents a benchmark to validate the mean current structure simulated in ORCA025-G70. Here the method used to compute the MOC transport follows that of *Lherminier et al.* [2010]. Potential density referenced to 1000 m (σ_1) is used instead of depth as a vertical coordinate to avoid a compensation effect, which would result from the East Greenland Irminger Current transporting cold waters at the same depth as the warm and northward NAC. The plane-normal velocity field is hence integrated from Greenland to Portugal within discrete isopycnal layers, before being summed vertically from the ocean bottom to be consistent with [*Lherminier et al.*, 2010]. The resulting overturning stream function is labeled as MOC$_\sigma$ hereafter. The density surface associated with the maximum of MOC$_\sigma$ (referred to as σ_{MOC} hereafter) delimits the upper and lower limbs of the overturning (referred to as MOC$_{UPPER}$ and MOC$_{LOWER}$ hereafter). Hence, the MOC$_\sigma$ intensity corresponds to the integrated transport of MOC$_{LOWER}$, which slightly differs from the integrated transport of MOC$_{UPPER}$ due to a nonzero net transport across the section, which presumably occurs within the upper layers (about 1 Sv in *Lherminier et al.* [2010]).

[15] The mean vertical structure of the simulated MOC$_\sigma$ at A25-Ovide for the period 1965–2004 is plotted in Figure 3a (solid colored lines). In ORCA025-G70, the maximum value amounts to 16 Sv with a mean σ_{MOC} positioned at $\sigma_1 = 32.09$, which is in line with typical overturning estimates in the northeastern Atlantic from eddy-permitting models [e.g., *Marsh et al.*, 2005; *Treguier et al.*, 2006] and observations [*Lherminier et al.*, 2010] (15 $\pm$ 1 Sv at $\sigma_1 = 32.14$, dashed line in Figure 3a). The maximum MOC$_\sigma$ in ORCA025-G70 is slightly lighter and stronger than the observed one, possibly due to the different averaging periods considered [*Treguier et al.*, 2006] and/or model errors. The net transport across the section amounts to 1 Sv, which is consistent with recent estimates of the Arctic mass balance [*Maslowski et al.*, 2004; *Cuny et al.*, 2005; *Serreze et al.*, 2006]. Also shown in Figure 3a is the mean vertical structure of the MOC$_\sigma$ at the Greenland-Scotland sills as seen in ORCA025-G70. The transports of its lower and upper branches are delimited by $\sigma_1 = 32.2$ and respectively refer to the intensity of the deep overflows (5 Sv) and of the net Atlantic inflow toward the Nordic Seas (6 Sv). The overflows are equally partitioned between the Denmark Strait (2.5 Sv) and the Iceland-Scotland passage (2.5 Sv). The Atlantic inflow above the Iceland-Feroe sill and the

(a)

(b)
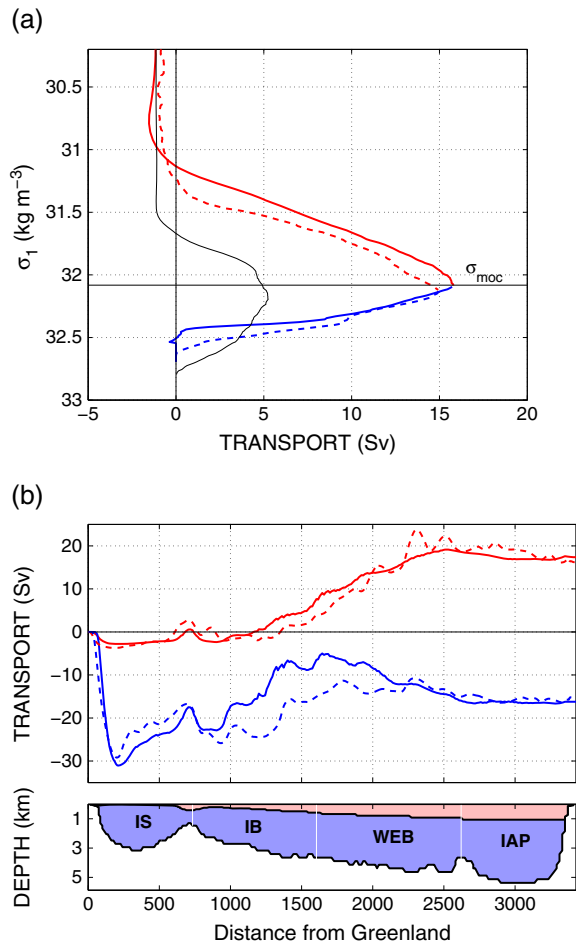
Figure 3. (a) Mean (1965–2004) vertical structure of the MOC$_\sigma$ at A25-Ovide (solid colored line). The mean velocity field has been integrated in density layers (0.01 kg m^{-3} resolution) and accumulated from the bottom (the transport sign has been inverted for clarity, so that the MOC$_\sigma$ intensity stands as a positive variable). The horizontal line indicates the density of the MOC$_\sigma$ maximum that delimits the MOC$_\sigma$ upper (red) and lower (blue) limbs (σ_{MOC} = 32.09). An observational estimate of the MOC$_\sigma$ vertical structure based on five hydrographic surveys (summer 2002, 2004, 2006, 2008, and 2010) is shown with a dashed line (Daniault, pers. comm., 2012). The thin black line is the vertical structure of the MOC$_\sigma$ at the Greenland-Scotland sills, computed in the same manner as for the A25-Ovide section. (b) The upper panel shows the mean horizontal structure of the upper (red) and lower (blue) MOC$_\sigma$ limbs at A25-Ovide in ORCA025-G70 (solid lines) and observations (dashed lines). Transports have been accumulated from Greenland such that an increasing (decreasing) transport denotes a northward (southward) flow. The lower panel shows the coarse bathymetric features of the section and the two-dimensional position of σ_{MOC}. The four distinct basins discussed in the text are labeled as: IS (Irminger Sea), IB (Iceland Basin), WEB (West European Basin) and IAP (Iberian Abyssal Plain).

Feroe-Scotland sill amounts to 2 and 4 Sv, respectively. The model slightly underestimates the water mass exchanges between the Nordic Seas and the North Atlantic relative to observations. For instance, *Hansen and Østerhus* [2000]

and *Østerhus et al.* [2005] estimated the mean overflow intensity at 6 Sv.

[16] The bathymetry of the A25-Ovide section is shown in Figure 3b along with the mean horizontal structures of the simulated and observed MOC$_\sigma$ limbs. The model realistically reproduces the horizontal features of the observed MOC$_{gma}$ limbs. The upper limb (red lines) presents a simple horizontal structure. It includes the lightest part of the southward flowing East Greenland Current (labeled as EGC hereafter, 3 Sv west of the 100 km) and the lightest part of the southward recirculation in the Iberian Abyssal Plain (labeled as REC hereafter, 3 Sv east of the 2500 km), which surround a strong northward transport in the Iceland Basin and West European Basin (23 Sv). This northward component of MOC$_{UPPER}$ is used as a proxy for the NAC transport hereafter. An anticyclonic recirculation occurs above Reykjanes Ridge, as shown in previous observational studies [*Bower et al.*, 2002; *Reverdin et al.*, 2003; *Flatau et al.*, 2003]. The net transport of MOC$_{UPPER}$ is 17 Sv, out of which 6 Sv cross the Greenland-Scotland sills and reach the Nordic Seas (Figure 3a). This means that 11 Sv of Atlantic waters are converted into intermediate and deep water masses in the Irminger and Iceland basins before leaving the ESPG within MOC$_{LOWER}$. These densified water masses merge with 5 Sv of deep overflow waters and 15 Sv of recirculating water from the Irminger and Iceland basins to form the narrow and intense boundary current along the Greenland continental slope (31 Sv). This quantitative picture of the basin wide volume transport and water mass transformation in the ESPG is in line with a recent estimate of the mean circulation between Cape Farewell and Iceland derived from hydrography and altimetry data [*Sarafanov et al.*, 2012].

3.2. The Lagrangian Analysis

[17] The use of the Lagrangian analysis tool will enable quantification of the transport of MOC$_{UPPER}$ according to the spatial origins of the involved water masses (subtropics and Labrador Sea). The experiments are performed offline within a domain bounded by the A25-Ovide section, a subpolar transect at the exit of the Labrador Sea (SPG section) and a subtropical transect at 39°N (STG section) (Figure 1). Every month between 1965 and 2003, about 300,000 numerical particles are initially positioned along A25-Ovide and above the time-dependent position of σ_{MOC}. Note that using a constant σ_{MOC} value (σ_1 = 32.09) yields very similar results. The numerical particles are advected freely by the three-dimensional model velocity field (i.e., the density criterion is only applied along the A25-Ovide section), and their trajectories are integrated until they leave the domain through one of the three defined sections (STG, SPG, or A25-Ovide). To fully reproduce the transport of MOC$_{UPPER}$, two different runs are needed: a temporal backward integration to quantify the northward (positive) flow across A25-Ovide (*EXP*$_{BACK}$), and a temporal forward integration to quantify the southward (negative) flow (*EXP*$_{FOR}$). The combined sum of the individual particle transports from both runs yields the total transport of MOC$_{UPPER}$ at A25-Ovide. Annual mean fields are then constructed from these monthly experiments. In *EXP*$_{BACK}$, the integration is done during a 7 year period to ensure that a large majority of particles ultimately reach a final section (only 1% of the initial particles stay within the domain, on average). This maximum travel time is reduced to 1 year for the *EXP*$_{FOR}$

experiment due to the much smaller distances travelled by the forward particles (see below), which on average reach a final section within one year. Due to the forward integration, the year 2004 is not considered in the following Lagrangian study. Two particle classes are then identified. The "local" class comprises the particles that recirculate back toward A25-Ovide through local recirculations (around Reykjanes Ridge for instance) or as part of the mesoscale eddy field. As seen in section 4.2, this class of particles has a null signature on the long-term average circulation but might be involved in the variability. The "remote" class comprises those particles that crossed either the STG or the SPG transects and thus refers to the large-scale oceanic flow. The "remote" versus "local" decomposition of the flow may be an original means to study eddy fluxes in higher resolution models. Here, we will only concentrate on the large-scale component of the circulation.

[18] Four "remote" components are extracted and their respective mean horizontal stream functions are plotted in Figure 4. EXP_{BACK} isolates the subtropical (Figure 4a, T_{STG} hereafter) and subpolar (Figure 4b, T_{SPG} hereafter) components of MOC_{UPPER} from the Gulf Stream and the Labrador Current, respectively. Their respective mean transports amount to 15 and 8 Sv and they jointly compose the NAC. This mean decomposition of the NAC transport is in line with the synthesized circulation scheme of *Schmitz and McCartney* [1993] and *Böning et al.* [1996]. EXP_{FOR} quantifies the transport of the upper fraction of the East Greenland Current around Cape Farewell (Figure 4c, T_{EGC} hereafter) and that of the southward recirculation in the Iberian Abyssal Plain that feeds the eastern limb of the

subtropical gyre (Figure 4d, T_{REC} hereafter). As already mentioned in the previous section, their mean transports amount to 3 Sv each.

[19] The present Lagrangian experiments enable us to consider the horizontal distribution of the MOC_{UPPER} components along A25-Ovide, as well as their respective hydrographic properties at A25-Ovide and in their source regions. Figure 5a shows the mean transport of the MOC_{UPPER} components summed horizontally along the A25-Ovide line. The most important feature arising from this representation is the equal contribution of T_{STG} and T_{SPG} to the NAC transport north of 49°N. This suggests that the water masses originating from the subtropical and subpolar sections have mixed and share similar hydrographic properties at A25-Ovide. To further illustrate this point, the salinity signatures of the MOC_{UPPER} components at the STG and SPG sections and at A25-Ovide are displayed in Figures 5b and 5c, respectively. Due to the small distances travelled by the forward particles, T_{EGC} and T_{REC} do not significantly change their salinity signature between A25-Ovide and the SPG and STG sections, respectively. By contrast, the salinity content of T_{STG} (T_{SPG}) substantially decrease (increase) as the particles travelled from the STG (SPG) section to the A25-Ovide section. While T_{STG} and T_{SPG} have very distinct salinity signatures in their source regions ($35 < S < 36.5$ and $S < 35$, respectively), they occupy the same salinity range at A25-Ovide ($34.7 < S < 36$) and form a relatively homogenous water mass (a similar result is found when using temperature instead of salinity). This confirms the strong mixing of both source waters as they flow within the NAC from Flemish Cap to the ESPG.
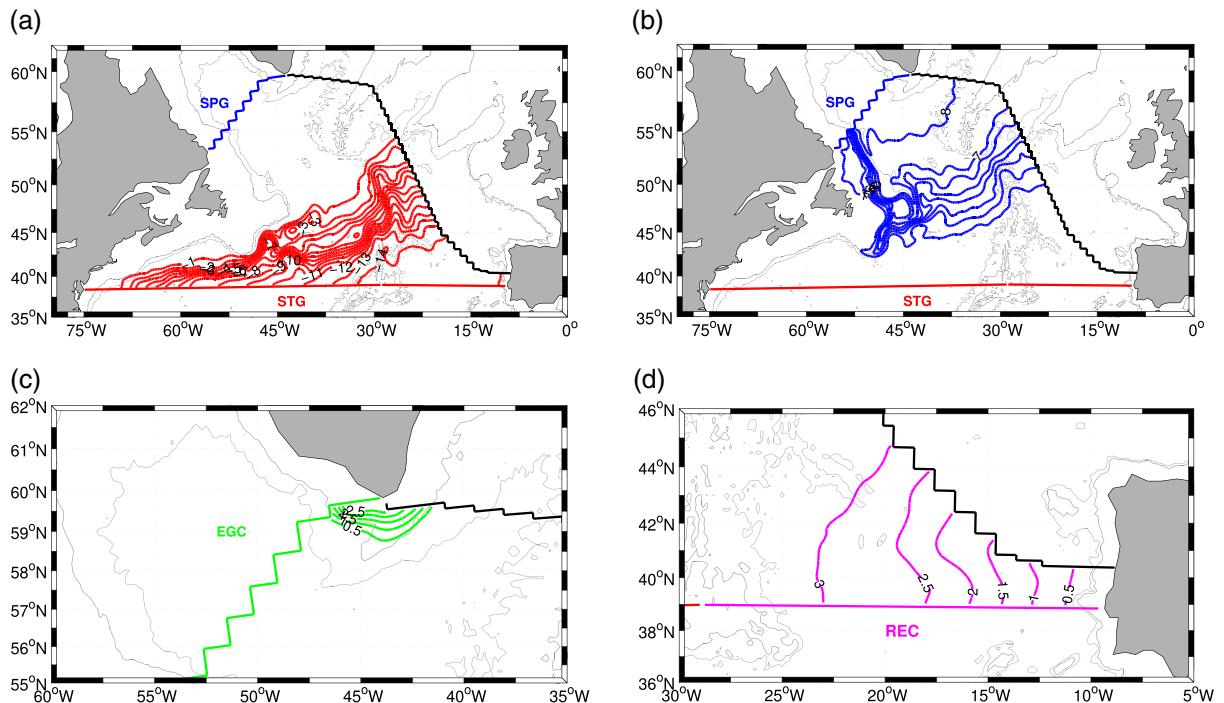
Figure 4. Mean (1965–2003) horizontal stream function (Sv) of the four "remote" components contributing to the MOC_{UPPER} transport across A25-Ovide: (a) the subtropical transport (T_{STG}), (b) the subpolar transport (T_{SPG}), (c) the EGC transport (T_{EGC}), and (d) the "Recirculation" transport (T_{REC}). Contour interval is 1 Sv in Figures 4a and 4b and 0.5 Sv in Figures 4c and 4d.
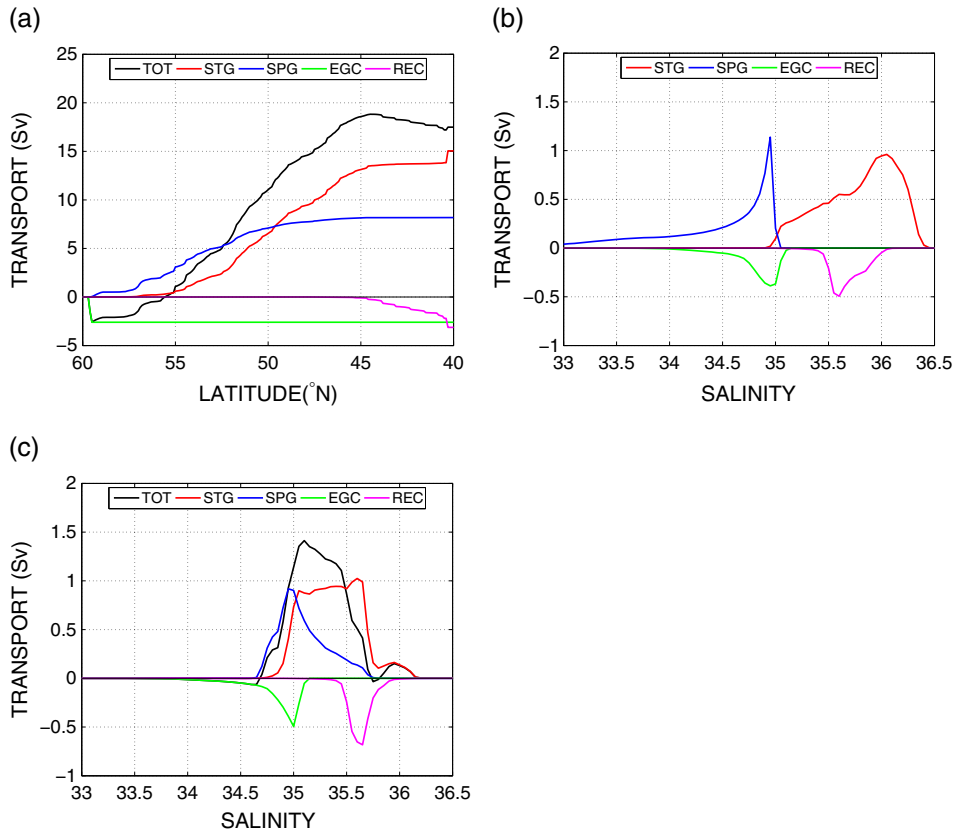
Figure 5. Mean (1965–2003) transport distributions (Sv) of the four "remote" components contributing to the MOC_{UPPER} transport as a function of (a) latitude at A25-Ovide (accumulated from Greenland), (b) salinity measured at the STG and SPG sections, and (c) salinity at A25-Ovide. In Figures 5b and 5c, the particle transports for each components were summed into $\delta S = 0.125$ salinity bins.

[20] While the subtropical contribution to MOC_{UPPER} (15 Sv) originates in the Gulf Stream, the subpolar inflow from the Labrador Current (8 Sv) may have two distinct origins: the Arctic outflow via Davis Strait and the western boundary current exiting the Irminger Sea and flowing cyclonically around the Labrador Sea. According to Figure 4c, we already know that the latter comprises 3 Sv of EGC waters flowing above σ_{MOC} at A25-Ovide. To quantify the origin of the remaining 5 Sv, we conducted an additional Lagrangian experiment (using the outputs from EXP_{BACK}) and decomposed T_{SPG} as the sum of three contributions: from Davis Strait (T_{SPG}^{Davis}), from the EGC above σ_{MOC} (T_{SPG}^{egc}), and from the DWBC off Greenland below σ_{MOC} (T_{SPG}^{dwbc}). Figure 6 provides a quantification of the transports and a schematic of the upper and lower circulations deduced from the results previously described. The mean T_{SPG}^{Davis}, T_{SPG}^{egc}, and T_{SPG}^{dwbc} amount to 1, 3, and 4 Sv, respectively. Importantly, 4 Sv of the dense waters formed north of A25-Ovide and leaving the ESPG via MOC_{LOWER} feed back into MOC_{UPPER} via the Labrador Current instead of being exported toward the subtropics. The mean MOC_σ intensity at A25-Ovide (16 Sv) integrates two distinct patterns of circulation: an overturning cell connecting the western and eastern subpolar gyres (4 Sv) and a subtropical overturning connecting low- and high-latitude regions (12 Sv). The subpolar overturning implies a decrease in density of dense water masses in the northwestern Atlantic. To investigate in detail the involved mechanisms requires a complete study of air-sea interaction and mixing along the western margin of the subpolar gyre, which is beyond the scope of the present study. We can however infer from our Lagrangian results the spatial pattern of this dense-to-light conversion (Figure 7). Density changes along the mean stream function of T_{SPG}^{dwbc} show an abrupt decrease in density in the vicinity of Flemish Cap, which is the region where the cold Labrador Current meets the warmer subtropical inflow from the Gulf Stream. Lateral mixing between the two source waters is likely important, as already noted from Figures 5b and 5c.

4. Variability of MOC_σ

[21] We here focus on the interannual to decadal variability of the MOC_σ at A25-Ovide for the period 1965–2004. The link between the strength of the MOC_σ and the horizontal structure of its upper limb is investigated. An Eulerian analysis is presented first and is then complemented via the Lagrangian experiment results.
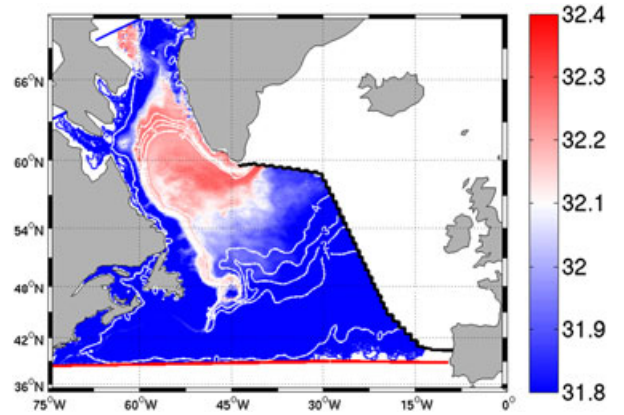
4.1. The Eulerian View

[22] Transport anomalies of the annual maximum MOC_σ relative to the long-term mean (1965–2004) are presented in Figure 8. The decadal variability is characterized by three noticeable periods: a weakening of the circulation by 2.5 Sv between 1965 and 1974, a strong intensification by 4 Sv between 1974 and 1995, and a sharp decline of 3.6 Sv
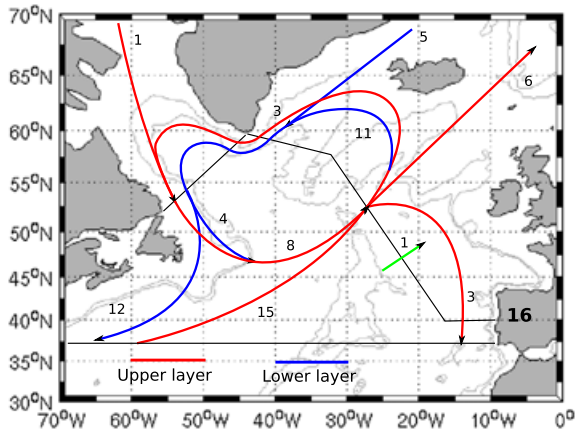
Figure 6. Schematic of the upper and lower circulation in the subpolar gyre deduced from Eulerian and Lagrangian diagnostics in ORCA025-G70 (in Sv). Red (blue) lines refer to the flow above (below) the mean σ_{MOC} value at A25-Ovide ($\sigma_1 = 32.09$). The green arrow indicates the net transport across the section. The bold 16 Sv value indicates the mean MOC_{σ} intensity at A25-Ovide. The NAC advects 15 Sv of subtropical waters (T_{STG}) and 8 Sv of subpolar waters (T_{SPG}) within the MOC_{UPPER}. Out of these 23 Sv, 6 Sv recirculate within the upper limb via T_{REC} (3 Sv) and T_{EGC} (3 Sv), while 1 Sv is exported toward the Arctic Ocean. The remaining 16 Sv are densified in the Nordic Seas (5 Sv) and in the ESPG (11 Sv) and leave the region within MOC_{LOWER}. A fraction (4 Sv) of these dense water masses decreases its density in the vicinity of Flemish Cape and feeds back into MOC_{UPPER} at A25-Ovide, while the remaining 12 Sv are exported toward the subtropics.

Figure 7. Mean (1965–2003) stream function (Sv) of T_{SPG}^{dwbc} (white lines, contour intervals of 1 Sv), superimposed on the associated mean particle density field (kg m^{-3}). The color bar is centered at $\sigma_1 = 32.09$ that is the mean σ_{MOC} value at A25-Ovide.

between 1995 and 2004. Although such low-frequency signal in the MOC_{σ} strength cannot be easily detected in observations, it is consistent with the transport index proposed by *Curry and McCartney* [2001] that describes a gradual weakening of the NAC during the 1960s followed by a significant intensification between 1970 and up to 1996 and a rapid slow-down until 2003 [*Kieke et al.*, 2007]. Those three major trends also appear in line with similar diagnosis performed in a wide range of OGCM experiments [e.g., *Marsh et al.*, 2005; *Bentsen et al.*, 2004; *Wunsch and Heimbach*, 2006; *Biastoch et al.*, 2008; *Huang et al.*, 2012]. The decadal variability of the MOC_{σ} evaluated across the Greenland-Scotland sills is relatively small (thin line in Figure 8), confirming that decadal changes of MOC_{σ} at A25-Ovide reflect the changing rate of water mass transformation in the ESPG rather than transport changes originating in the Nordic Seas. This is either atmospherically-driven or internally-driven via entrainment downstream of the sills.

[23] To investigate the link between the MOC_{σ} variability and the changing horizontal structure of the NAC current system, we show in Figure 9a the difference in the cumulative horizontal transport of MOC_{UPPER} between two distinct periods characterized by opposing MOC_{σ} states (see gray shading in Figure 8): 1987–1997 (strong) minus 1968–1978 (weak). In this representation, an upward (downward) slope within a given latitudinal range indicates a stronger (weaker) transport in 1987–1997 than in 1968–1978. Opposite latitudinal changes occurred on each sides of 49°N between the two

periods. Volume transports on each side of 49°N can be interpreted as the intensity of the northern and southern NAC branches that feed the Iceland basin and the Rockall Trough, respectively (*Lherminier et al.*, 2010). Note that 49°N is also a noticeable boundary for the mean composition of the NAC (see Figure 5a). Figure 9a implies that a strong MOC_{σ} state at A25-Ovide is associated with a relatively strong transport of the cold/fresh northern branch and a relatively weak transport of the warm/salty southern branch, and vice-versa for a weak MOC_{σ} state. Importantly, it is the respective intensities of the branches rather than a geographical shift in their positions that changes. In fact, the strongest velocity fronts in ORCA025-G70 keep a relatively fixed position over time [*De Boisséson*, 2010]. In the following section, the variability
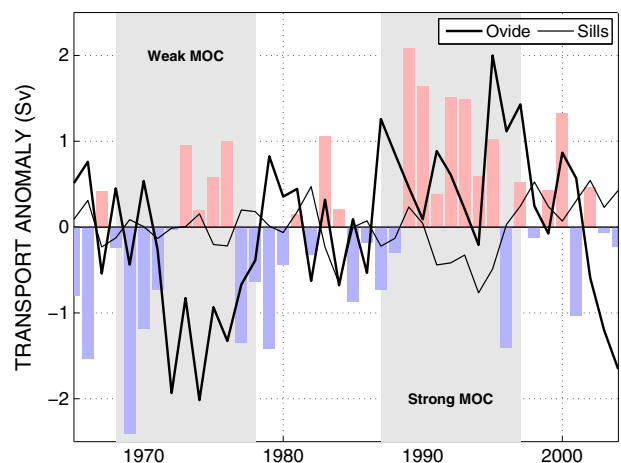
Figure 8. Annual transport anomalies of the MOC_{σ} across A25-Ovide (thick line) and across the Greenland-Scotland sills (thin line) relative to the mean of 1965–2004 (in Sv). The shaded areas denote two distinct periods respectively characterized by a weak (1968–1978) and a strong (1987–1997) MOC_{σ} state. The normalized winter NAO index is shown with bars (red: positive NAO years; blue: negative NAO years).

(a)

EULERIAN

(b)
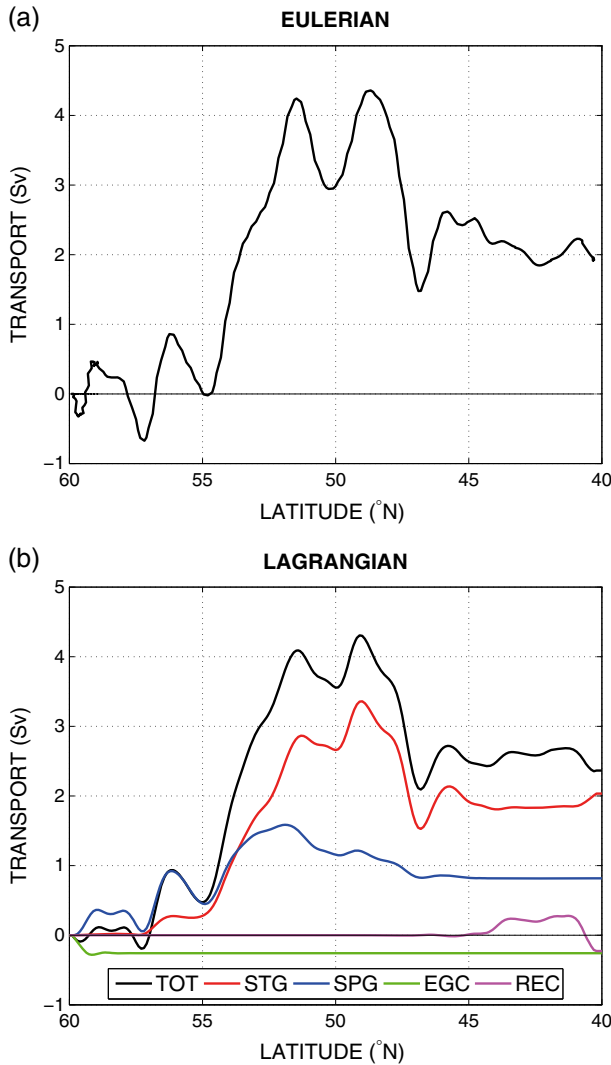
LAGRANGIAN

Figure 9. Changes in the latitudinal distribution of MOC$_{UPPER}$ (in Sv) between the strong (1987–1997) and the weak (1968–1978) MOC$_\sigma$ period depicted in Figure 8 for (a) the Eulerian calculation and (b) the Lagrangian reconstruction. The four remote components of MOC$_{UPPER}$ are shown as indicated in the legend. Transport anomalies have been accumulated from Greenland.

4.2. The Lagrangian Analysis

[24] The reconstructed transport anomalies of MOC$_{UPPER}$ in the Lagrangian framework agrees well with the Eulerian transport signal (Figure 10a). The small differences between the transports on interannual timescales result from the precision of the Lagrangian transport calculation (a small fraction of the numerical particles do not reach any final section within the allocated integration time). Note here that the transport index of MOC$_{UPPER}$ includes the contribution from the net transport variability, and is hence slightly different than the actual maximum MOC$_\sigma$ signal described in Figure 8. Figure 10b displays the respective contributions

of the "remote" and the "local" components of the circulation (see section 3.2). Although both signals share a weak anticorrelation ($r = -0.3$), most of the decadal signal is explained by the "remote" component, and hence the "local" contribution will be neglected hereafter.

[25] Figure 11 shows the respective contributions of T_{STG}, T_{SPG}, T_{REC}, and T_{EGC} to the total transport changes of MOC$_{UPPER}$. The variability of the southward components of MOC$_{UPPER}$ (T_{REC} and T_{EGC}, Figures 11a and 11b, respectively) contains no substantial decadal signal. Their respective transport anomalies cannot be neglected on interannual timescales, though. A significant anti-correlation is found between T_{REC} and T_{STG} ($r = -0.6$). This corroborates that the southward recirculation in the Iberian abyssal plain is closely related to the interannual variability of subtropical water transport carried out by the NAC, as proposed in recent observational and modeling studies [*Treguier et al.*, 2006; *Gourcuff*, 2008; *Lherminier et al.*, 2010]. Interestingly, the two components of the NAC (T_{STG} and T_{SPG}, Figures 11c and 11d,

(a)

(b)
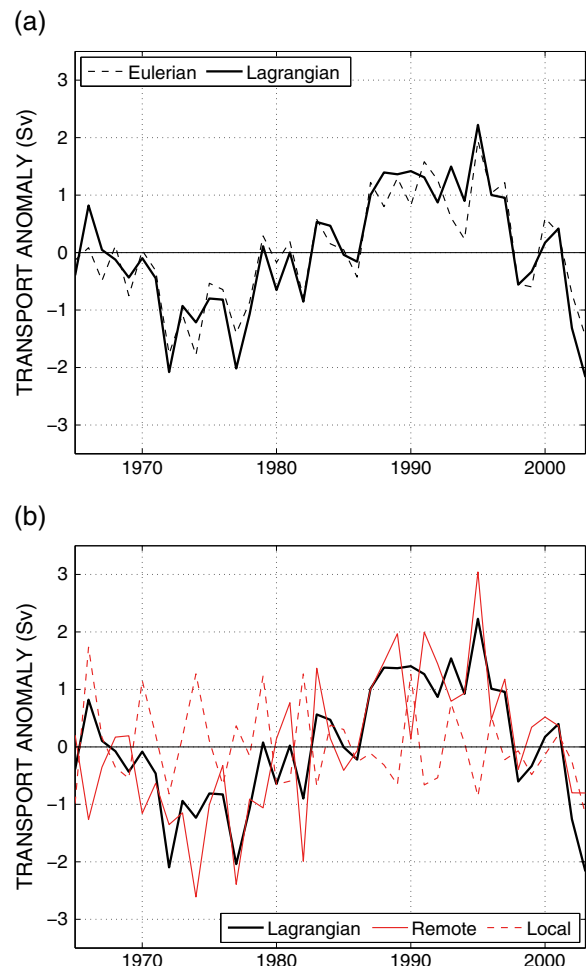
Figure 10. (a) Annual transport anomaly (Sv) of MOC$_{UPPER}$ relative to the mean of 1965–2003 for the Eulerian calculation (thin dashed line) and Lagrangian reconstruction (thick solid line) including the "remote" and the "local" contributions. (b) The same as Figure 10a, but with the Lagrangian transport decomposed into its "remote" (solid red line) and "local" (dashed red line) parts.
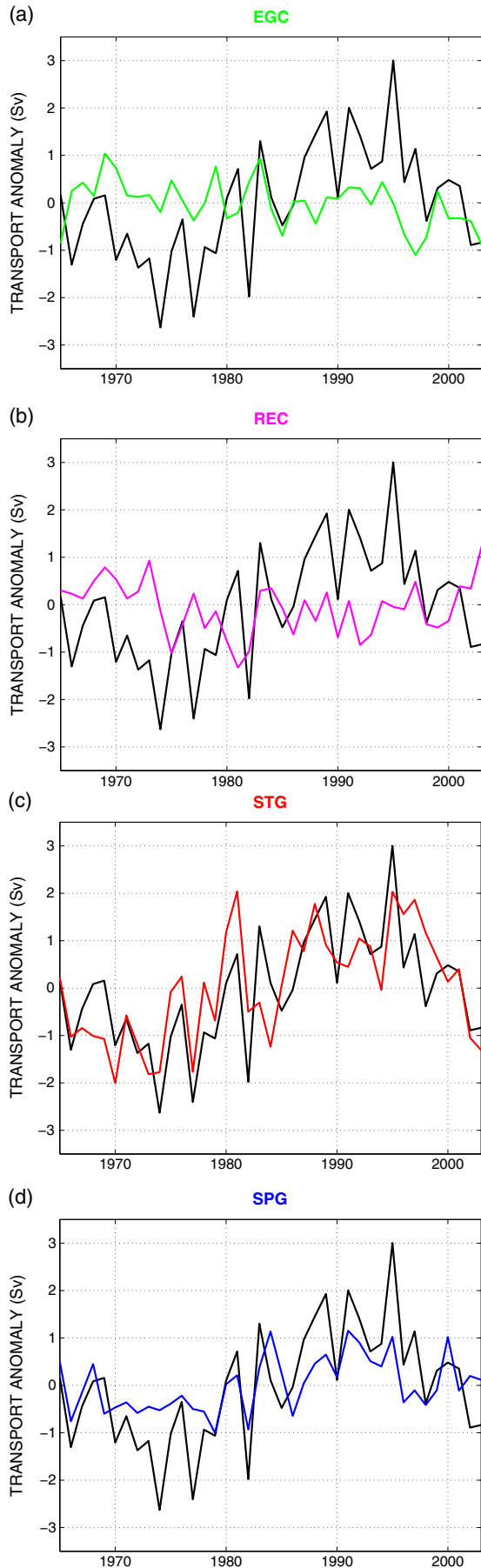
signals previously described are assessed from a Lagrangian point of view, with a focus on changing transports associated with the subtropical and subpolar components of the NAC.

respectively) exhibit similar decadal behaviors with an amplitude corresponding to ~25% of their respective mean transports. Both components present a decreasing transport in the 1960–1970s followed by a gradual intensification until the mid-1990s and a decline afterwards. The two components are strongly correlated on decadal timescales ($r = 0.8$ when both signals are 10 year low-pass filtered). As a consequence, the proportion of subpolar and subtropical waters crossing the section within the NAC remains relatively constant on decadal timescales. In particular, the strong and weak MOC_σ phases of the 1990s and 1970s are characterized by the same proportion of subtropical (65%) and subpolar (35%) waters within the NAC. Over the 1965–2004 time period, the $T_{STG}/(T_{STG} + T_{SPG})$ ratio fluctuates between 60% and 68% and those fluctuations show no correlation with the variability of the NAC (not shown).

[26] As highlighted from the Eulerian diagnosis (Figure 9a), the difference between a weak and a strong MOC_σ state across the A25-Ovide section is characterized by opposed changes north and south of ~49°N. In the Lagrangian experiments (Figure 9b), the transport changes on either sides of this latitudinal boundary are dominated by changes in the subtropical transport. Most importantly, T_{STG} accounts for about 70% of the total transport change between 49°N and 58°N, that is within the relatively cold and fresh Iceland Basin. The subpolar contribution cannot be neglected though, and dominates the transport changes north of 55°N.

[27] In summary, the decadal variability of MOC_{UPPER} is largely linked to the NAC variability ($r = 0.86$), which reflects in-phase changes of the subtropical and subpolar transports. Additionally, the changing horizontal structure of the NAC transport between two persistent and opposed states of the MOC_σ is associated with opposite variability of its main branches, primarily induced by subtropical transport changes.

5. On the Link Between the Intensity and the Spatial Extent of the Subtropical Inflow

[28] In a recent study based on numerical tracer experiments performed with the Simple Ocean Assimilation System, *Häkkinen et al.* [2011] highlighted significant changes in the spatial extent of subtropical water masses in the northeastern Atlantic with potential effect on the salinity content of the ESPG. Three periods of increased connection between the Gulf Stream waters and the ESPG were observed: the late 1960s, the 1980s, and the early 2000s. The authors suggested an impact of those penetration events on the composition of the upper MOC_σ limb in middle- to high-latitude regions, but the link with the actual strength of the overturning cell remains obscure.

[29] An additional set of Lagrangian experiments was conducted to relate our quantitative estimates of the subtropical contribution to the MOC_σ variability at A25-Ovide (i.e.,

Figure 11. Annual transport anomaly (Sv) relative to the mean of 1965–2003 for the four MOC_{UPPER} components (colored lines) superimposed on the total MOC_{UPPER} transport anomaly (black). Positive anomalies for the T_{STG} and T_{SPG} (T_{EGC} and T_{REC}) refer to an intensified (weakened) northward (southward) transport across A25-Ovide.

T_{STG}) with a qualitative estimate of changes in the spatial extent of subtropical water masses. Each month between 1965 and 2004, artificial particles were distributed every 0.5° of longitude along the STG transect at several depth levels between the surface and 1200 m depth (a total number of 1560 particles were released each year at each depth level). The particles were then allowed to evolve freely within the model velocity field during 3 years. This particular advection time ensures that particles have enough time to reach the ESPG. We show in Figure 12a the resulting subtropical trajectories of particles released at the sea surface in 2001. One can note that a large majority of particles recirculated within the subtropical gyre south of 40°N while a relatively small proportion reached high latitude regions. This appears consistent with the very weak intergyre connections captured by observational surface drifters [*Brambilla and Talley*, 2006; *Häkkinen and Rhines*, 2009]. To provide a temporally continuous quantification of intergyre exchanges within the upper water column, the number of numerical particles located east of the A25-Ovide line during each year was quantified. The resulting index is considered as a proxy for the northeastward extent of subtropical water masses, at each depth level (note that this index is not a volume transport index but a "penetration" index). It is displayed as a Hovmöller diagram in Figure 12b.

The strongest intergyre connection occurs below the surface (at 300 m depth here) and relatively weak connection is seen at the surface. This is consistent with the recent study of *Burkholder and Lozier* [2011] who combined an eddy-resolving OGCM and artificial Lagrangian floats to highlight the strong subsurface signature of intergyre exchanges in the North Atlantic. The three major periods of increased intrusion of subtropical waters toward the ESPG pointed out in the Simple Ocean Assimilation System by *Häkkinen et al.* [2011] are particularly well reproduced: the late 1960s, the 1980s, and the early 2000s. Note also that relatively high values are observed around 1990. The (normalized) penetration index averaged within the 0–400 m layer is compared in Figure 12c with the volume transport anomalies of T_{STG} at A25-Ovide (see Figure 11c). Both time series, which can respectively be related to the northeastward extent and the strength of the subtropical contribution to the NAC/MOC$_{UPPER}$ transport, are anticorrelated ($r = -0.55$). This is particularly evident during the well-documented period of the late 1990s to early 2000s: an intense weakening of the subtropical transport within the NAC occurred in concomitance with an enhanced intrusion of subtropical water in the ESPG. Investigating this causal relationship is beyond the scope of the present paper, and we here simply conclude that the northeastward extent of subtropical water masses toward
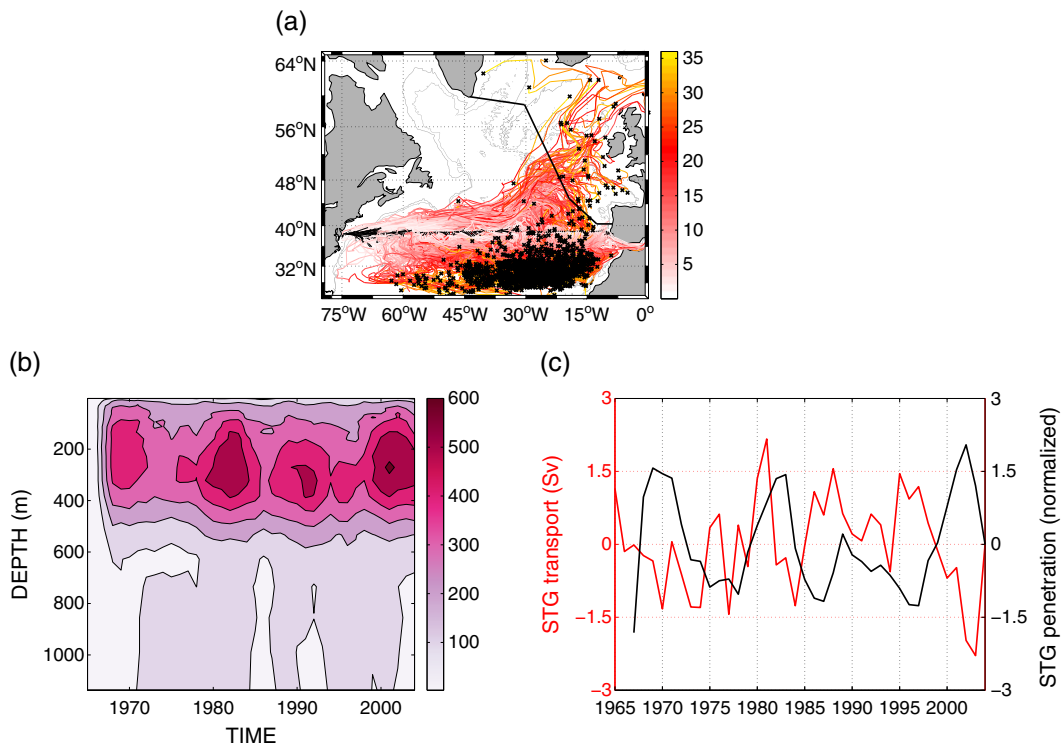
Figure 12. (a) Trajectories of 1560 numerical particles launched at the surface in 2001 along the STG transect and advected within the model velocity field during 3 years. Colors indicate the age of particles in month and black crosses indicate the particle final positions. (b) Hovmöller diagram of the normalized index of the northeastward penetration of subtropical waters in the ESPG. The index corresponds to the number of numerical particles located east of A25-Ovide during each year, as a function of launch depth from the STG line. (c) Same as Figure 12b but average within the 0–400 m layer (black line). The volume transport anomalies associated with the subtropical component of MOC$_{UPPER}$ (T_{STG}) are shown in red. Both time series have been detrended.

the ESPG describes an out-of-phase relationship with the actual subtropical volume transport variability, especially from 1985 onward.

6. Discussion

[30] The described variability of the NAC/MOC$_\sigma$ in ORCA025-G70 is globally consistent with the decadal NAO signal (see Figure 8). When considering the low-frequency part of both time series (10 year low-pass filtering), the NAO leads the MOC$_\sigma$ at A25-Ovide by 4–5 years ($r = 0.7$). Interestingly, the MOC$_\sigma$ and NAC indexes at A25-Ovide show a clear correspondence with a baroclinic intergyre transport index computed from hydrographic data collected at Bermuda and at station *Bravo* in the Labrador Sea [*Curry and McCartney*, 2001; *Kieke et al.*, 2007]. This observational index of the NAC transport was shown to lag the NAO fluctuations by 2–3 years. The greater lag found at A25-Ovide in the model is consistent with the mean travel time needed by the numerical particles to reach the ESPG from the Labrador Sea or the subtropics (about 2 years). Moreover, *Curry and McCartney* [2001] showed that the subtropical and subpolar gyre intensities fluctuate in phase on decadal timescales, in good agreement with our Lagrangian results (see Figure 11).

[31] Changes in the horizontal shape of the upper layer transport at A25-Ovide (see Figure 9) might reflect meridional shifts of the zero wind-stress curl line associated with the NAO low-frequency signal. Anomalous Ekman pumping is thought to create an anomalous gyre circulation at midlatitudes, often referred to as the intergyre gyre [*Marshall et al.*, 2001]. It can be identified as the subtropical pole of variability in the gyre index spatial structure (see Figure 2). During high NAO conditions, this intergyre gyre is anticyclonic, and tends to increase (decrease) the transport of the northern (southern) NAC branch. *Herbaut and Houssais* [2009] pointed out this wind-driven anomalous circulation as an important contributor to the changing structure of the NAC and associated changes in the salinity content of the ESPG. On the other hand, our "penetration" index, reflecting the northeastward intrusion of warm subtropical waters in the ESPG, shows no significant correlation with the NAO index at the 95% level. In fact, *Häkkinen et al.* [2011] suggested that those episodes of increased intergyre connection in the northeastern Atlantic reflect a modulation of the climatological wind stress curl field, which is only weakly correlated with the NAO index.

7. Conclusion

[32] Decadal changes of the overturning circulation in the density space at A25-Ovide have been quantified in the ORCA025-G70 simulation for the 1965–2004 period. The mean structure and intensity of the MOC$_\sigma$ were in line with observations and its variability was shown to sustain substantial decadal signals in good agreement with previous observational and modeling studies. A transport index of the upper MOC$_\sigma$ limb across the A25-Ovide section was constructed from a set of Lagrangian experiments. The respective impacts of the subtropical and subpolar inflow variability on the strength and spatial structure of the NAC were of particular interest. The variability of the subtropical volume transport within the NAC was further compared to a qualitative index of the northward intrusion of subtropical water masses in the ESPG. Accordingly, we reach the following conclusions:

[33] 1. The time-averaged MOC$_\sigma$ across A25-Ovide (16 Sv) can be decomposed into a subtropical cell connecting low- and high-latitude regions (12 Sv) and a cell internal to the subpolar gyre (4 Sv). The MOC$_\sigma$ decadal variability is associated with an in-phase relationship between the subtropical and the subpolar components of the NAC.

[34] The NAC forms the main component of the upper MOC$_\sigma$ limb in the ESPG. Its mean transport is composed of two thirds of subtropical waters from the Gulf Stream (15 Sv) and one third of subpolar water masses from the Labrador Current (8 Sv). Half of the subpolar contribution (4 Sv) is associated with a dense-to-light conversion of deep western boundary current waters. The Lagrangian experiments indicate that this decrease in density primarily occurs in the vicinity of Flemish Cap, where subpolar water masses meet the warm Gulf Stream waters. Strong lateral mixing was consistently observed in this particular region [e.g., *Dutkiewicz et al.*, 2001; *Perez-Brunius et al.*, 2004]. Overall, the cyclonic subpolar gyre circulation contributes to a quarter of the mean MOC$_\sigma$ at A25-Ovide (4 Sv out of 16 Sv). The remaining 12 Sv are carried out by a subtropical meridional cell advecting Gulf Stream waters in its upper limb. The maximum MOC$_\sigma$ variability evaluated at A25-Ovide describes a strong positive trend between the mid-1970s and the mid-1990s followed by a rapid weakening until the mid-2000s, and presumably relates to NAO-related forcing. The transport changes in the upper limb are predominantly related to the intensity of the NAC, which reflects an in-phase relationship between its subtropical and subpolar components. This is in line with the study of *Curry and McCartney* [2001] that showed coherent changes in the strength of the subtropical and subpolar gyre on decadal timescales. The relative proportion of the basin wide subtropical and subpolar transports within the upper MOC$_\sigma$ limb at A25-Ovide consequently shows no substantial decadal variations.

[35] 2. Decadal changes in the MOC$_\sigma$ strength at A25-Ovide are associated with horizontal restructuring of the NAC transport.

[36] Opposed transport changes on each side of ~49°N are noted. When the MOC$_\sigma$ is in a strong phase (1990s), the cold water transport within the Iceland Basin associated with the northern NAC branch is strong while the warm water transport of the southern branch at the Rockall Trough entrance is relatively weak (the inverse is true for a weak MOC$_\sigma$ phase as in the 1970s and 2000s). As shown through Lagrangian experiments, this spatial pattern of variability primarily reflects a redistribution of subtropical water masses within the NAC. This differs from the conclusion of *Hátún et al.* [2005] suggesting the subpolar gyre dynamics as the main driving mechanism behind the changing structure and composition of the NAC in the ESPG. This potential contradiction relies on the methods used to separate the subtropical and subpolar transport signatures within the NAC. We note here that the mean NAC transport north of 49°N is equally partitioned between waters of subpolar and subtropical origins (~7 Sv each), and that their respective signatures on the NAC variability can hence not be extracted hydrographically.

[37] 3. Periods of expanded subtropical gyre generally occur during periods of weak subtropical volume transport, and weak MOC$_\sigma$ in the northeastern Atlantic.

[38] Qualitative analysis of subtropical water trajectories enables us to continuously monitor the spatial extent of the subtropical gyre in the northeastern Atlantic. The three periods of increased connection between Gulf Stream waters and the ESPG highlighted in *Häkkinen et al.* [2011] were satisfactorily reproduced (late 1960s, around 1980, and early 2000s). The Lagrangian experiments enable us to link those penetration events with the intensity of the subtropical overturning cell. Both indices describe opposed behavior on interannual/ decadal timescales, in agreement with the recent suggestion of *Chaudhuri et al.* [2011]. A stronger (weaker) subtropical volume transport across A25-Ovide is generally associated with a weaker (stronger) northeastward intrusion of subtropical water masses in the ESPG.The present description of the MOC$_\sigma$ variability at A25-Ovide now needs to be considered in a heat/freshwater transport perspective. Heat transport was particularly shown to drive significant heat content changes on decadal timescales in the subpolar gyre [*Grist et al.*, 2010]. A heat budget investigation within the ESPG performed in a similar Eulerian/Lagrangian framework is part of an ongoing study.

References

Barnier, B., G. Madec, T. Penduff, J.-M. Molines, A.-M. Tréguier, J. L. Sommer, A. Beckmann, A. Biastoch, C. Böning, J. Dengg, C. Derval, E. Durand, S. Gulev, E. Remy, C. Talandier, S. Theetten, M. Maltrud, J. McLean, and B. D. Cuevas (2006), Impact of partial steps and momentum advection schemes in a global ocean circulation model at eddy-permitting resolution, *Ocean Dynamics*, *56*, 543–567, doi:10.1007/s10236-006-0082-1.

Bentsen, M., H. Drange, T. Furevik, and T. Zhou (2004), Simulated variability of the Atlantic meridional overturning circulation, *Clim. Dyn.*, *22*(6-7), 701–720, doi:10.1007/s00382-004-0397-x.

Bersh, M. (2002), North Atlantic Oscillation-induced changes of the upper layer circulation in the northern North Atlantic Ocean, *J. Geophys. Res.*, *107*(C10), 223–235, doi:10.1029/2001JC000901.

Bersh, M., I. Yashayaev, and K. P. Koltermann (2007), Recent changes of the thermohaline circulation in the subpolar North Atlantic, *Ocean Dynamics*, *57*(3), 223–235, doi:10.1007/s10236-007-0104-7.

Biastoch, A., C. W. Böning, and J. Getzlaff (2008), Causes of Interannual-Decadal Variability in the Meridional Overturning Circulation of the Midlatitude North Atlantic Ocean, *J. Clim.*, *21*(24), 6599–6615, doi:10.1175/2008JCLI2404.1.

Bingham, R. J., C. W. Hughes, V. Roussenov, and R. G. Williams (2007), Meridional coherence of the North Atlantic meridional overturning circulation, *Geophys. Res. Lett.*, *34*(L23606), doi:10.1029/2007GL031731.

Blanke, B., and S. Raynaud (1997), Kinematics of the Pacific Equatorial Undercurrent: An Eulerian and Lagrangian Approach from GCM Results, *J. Phys. Oceanogr.*, *27*(6), 1038–1053, doi:10.1175/1520-0485(1997)027 < 1038:KOTPEU > 2.0.CO;2.

Blanke, B., M. Arhan, G. Madec, and S. Roche (1999), Warm water paths in the equatorial Atlantic as diagnosed with a general circulation model, *J. Phys. Oceanogr.*, *29*(11), 2753–2768, doi:10.1175/1520-0485(1999)029 < 2753:WWPITE > 2.0.CO;2.

Böning, C., M. Scheinert, J. Dengg, A. Biastoch, and A. Funk (2006), Decadal variability of subpolar gyre transport and its reverberation in the North Atlantic overturning, *Geophys. Res. Lett.*, *33*(L21S01), doi:10.1029/2006GL026906.

Böning, C. W., F. O. Bryan, W. R. Holland, and R. Döscher (1996), Deep-water Formation and Meridional Overturning in a High-Resolution Model of the North Atlantic, *J. Phys. Oceanogr.*, *26*(7), 1142–1164, doi:10.1175/1520-0485(1996)026 < 1142:DWFAMO > 2.0.CO;2.

Bower, A. S., and W.-J. von Appen (2007), Interannual variability in the Pathways of the North Atlantic Current over the Mid-Atlantic Ridge and the Impact of Topography, *J. Phys. Oceanogr.*, *38*, 104–120, doi:10.1175/2007JPO3686.1.

Bower, A. S., B. L. Cann, T. Rossby, W. Zenk, J. Gould, K. Speer, P. L. Richardson, M. D. Prater, and H. M. Zhang (2002), Directly measured mid-depth circulation in the northeastern North Atlantic Ocean, *Nature*, *419*, 603–607, doi:10.1038/nature01078.

Brambilla, E., and L. D. Talley (2006), Surface drifter exchange between the North Atlantic subtropical and subpolar gyres, *J. Geophys. Res.*, *111*(C07026), doi:10.1029/2005JC003146.

Brambilla, E., and L. D. Talley (2008), Subpolar Mode Water in the northeastern Atlantic: 1. Averaged properties and mean circulation, *J. Geophys. Res.*, *113*(C04025), doi:10.1029/2006JC004062.

Brambilla, E., L. D. Talley, and P. E. Robbins (2008), Subpolar Mode Water in the northeastern Atlantic: 2. Origin and transformation, *J. Geophys. Res.*, *113*(C04026), doi:10.1029/2006JC004063.

Brodeau, L., B. Barnier, T. Penduff, A.-M. Tréguier, and S. Gulev (2009), An evaluation of ERA-40 and CORE atmospheric variables as drivers of global ocean models, *Ocean Modell.*, *31*, 88–104, doi:10.1016/j.ocemod.2009.10.005.

Burkholder, K. C., and M. S. Lozier (2011), Subtropical to subpolar pathways in the North Atlantic: Deductions from lagrangian trajectories, *J. Geophys. Res.*, *116*(C07017), doi:10.1029/2010JC006697.

Chaudhuri, A. H., A. Gangopadhyay, and J. J. Bisagni (2011), Contrasting response of the eastern and western North Atlantic circulation to an episodic climate event, *J. Phys. Oceanogr.*, *41*(9), 1630–1638, doi:10.1175/2011JPO4512.1.

Cuny, J., P. B. Rhines, and R. Kwok (2005), Davis Strait volume, freshwater and heat fluxes, *Deep Sea Res. I*, *52*(3), 519–542, doi:10.1016/j.dsr.2004.10.006.

Curry, R. G., and M. S. McCartney (2001), Ocean Gyre Circulation Changes Associated with the North Atlantic Oscillation, *J. Phys. Oceanogr.*, *31*, 3374–3400, doi:10.1175/1520-0485(2001)031 < 3374:OGCCAW > 2.0.

Daniault, N., P. Lherminier, and H. Mercier (2011a), Circulation and Transport at the southeast Tip of Greenland, *J. Phys. Oceanogr.*, *41*(3), 437–457, doi:10.1175/2010JPO4428.1.

Daniault, N., H. Mercier, and P. Lherminier (2011b), The 1992-2009 transport variability of the East Greenland Current at 60 degrees N, *Geophys. Res. Lett.*, *38*(L07601), doi:10.1029/2011GL046863.

de Boisséson, E. (2010), Les eaux modales du gyre subpolaire de l'Atlantique Nord: origine, formation, variabilité, Ph.D. thesis, Université de Bretagne Occidentale, htttp://archimer.ifremer.fr/doc/2010/these-7469.pdf.

de Boisséson, E., V. Thierry, H. Mercier, G. Caniaux, and D. Desbruyères (2012), Origin, formation and variability of the Subpolar Mode Water observed over the Reykjanes Ridge, *J. Geophys. Res.*, *117*, C12005, doi:10.1029/2011JC007519.

Deshayes, J., and C. Frankignoul (2008), Simulated Variability of the Circulation in the North Atlantic from 1953 to 2003, *J. Clim.*, *21*(19), 4919–4933, doi:10.1175/2008JCLI1882.1.

Dutkiewicz, S., L. Rothstein, and T. Rossby (2001), Pathways of cross-frontal exchange in the North Atlantic Current, *J. Geophys. Res.*, *106*(C11), 26,917–26,928, doi:10.1029/1999JC000089.

Eden, C., and T. Jung (2001), North Atlantic Interdecadal Variability: Oceanic Response to the North Atlantic Oscillation (1865-1997), *J. Clim.*, *14*(5), 676–691, doi:10.1175/1520-0442(2001)014 < 0676:NAIVOR > 2.0.CO;2.

Eden, C., and J. Willebrand (2001), Mechanism of Interannual to Decadal Variability of the North Atlantic Circulation, *J. Clim.*, *14*(10), 2266–2280, doi:10.1175/1520-0442(2001)014 < 2266:MOITDV > 2.0.CO;2.

Esselborn, S., and C. Eden (2001), Sea Surface Height changes in the North Atlantic Ocean related to the North Atlantic Oscillation, *Geophys. Res. Lett.*, *28*(18), 3473–3476, doi:10.1029/2001GL012863.

Fichefet, T., and M. A. M. Maqueda (1999), Modelling the influence of snow accumulation and snow-ice formation on the seasonal cycle of the Antarctic sea-ice cover, *Clim. Dyn.*, *15*(4), 251–268, doi:10.1007/s003820050280.

Flatau, M. K., L. Talley, and P. P. Niiler (2003), The North Atlantic Oscillation, Surface Current Velocity, and SST Changes in the Subpolar North Atlantic, *J. Clim.*, *16*, 2355–2369, doi:10.1175/2787.1.

Gourcuff, C. (2008), Etude de la variabilité de la circulation du Gyre Subpolaire de l'Atlantique nord à l'aide des données OVIDE et des mesures satellitaires., Ph.D. thesis, Université de Bretagne Occidentale, http://archimer.ifremer.fr/doc/2008/these-6226.pdf.

Gourcuff, C., P. Lherminier, H. Mercier, and P.-Y. L. Traon (2011), Altimetry Combined with Hydrography for Ocean Transport Estimation, *J. Atmos. Oceanic Technol.*, 28, 1324–1337, doi:10.1175/2011JTECHO818.1.

Griffies, S. M., A. Biastoch, C. Böning, F. Bryan, G. Danabasoglu, E. P. Chassignet, M. H. England, R. Gerdes, H. Haak, R. W. Hallberg, W. Hazeleger, J. Jungclaus, W. G. Large, G. Madec, A. Pirani, B. L. Samuels, M. Scheinert, A. S. Gupta, C. A. Severijns, H. L. Simmons, A.-M. Treguier, M. Winton, S. Yeager, and J. Yin (2009), Coordinated Ocean-ice Reference Experiments (COREs), *Ocean Modell.*, 26(1-2), 1–46, doi:10.1016/j.ocemod.2008.08.007.

Grist, J. P., S. A. Josey, R. Marsh, S. A. Good, A. C. Coward, B. A. de Cuevas, S. G. Alderson, A. L. New, and G. Madec (2010), The roles of surface heat flux and ocean heat transport convergence in determining Atlantic Ocean temperature variability, *Clim. Dyn.*, 60(4), 771–790, doi:10.1007/s10236-010-0292-4.

Gulev, S. K., B. Barnier, H. Knochel, J.-M. Molines, and M. Cottet (2003), Water Mass Transformation in the North Atlantic and Its Impact on the Meridional Circulation: Insights from an Ocean Model Forced by NCEP-NCAR Reanalysis Surface Fluxes, *J. Clim.*, 16(19), 3085–3110, doi:10.1175/1520-0442(2003)016 < 3085:WMTITN > 2.0.CO;2.

Häkkinen, S. (1999), Variability of the simulated meridional heat transport in the North Atlantic for the period 1951-1993, *J. Geophys. Res.*, 104(C5), doi:10.1029/1999JC900034.

Häkkinen, S., and P. B. Rhines (2004), Decline of the Subpolar North Atlantic Circulation During the 1990s., *Science*, 304(5670), 555–559, doi:10.1126/science.1094917.

Häkkinen, S., and P. B. Rhines (2009), Shifting Surface Current in the northern North Atlantic Ocean, *J. Geophys. Res.*, 114(C04005), doi:10.1029/2008JC004883.

Häkkinen, S., P. B. Rhines, and D. L. Worthen (2011), Warm and saline events embedded in the meridional circulation of the northern North Atlantic, *J. Geophys. Res.*, 116(C03006), doi:10.1029/2010JC006275.

Hansen, B., and S. Østerhus (2000), North Atlantic - Nordic Seas exchanges, *Prog. Oceanogr.*, 45(2), 109–208, doi:10.1016/S0079-6611(99)00052-X.

Hátún, H., A. B. Sandø, H. Drange, B. Hansen, and H. Valdimarsson (2005), Influence of the Atlantic Subpolar Gyre on the Thermohaline Circulation, *Science*, 309(5742), 1841–1844, doi:10.1126/science.1114777.

Herbaut, C., and M.-N. Houssais (2009), Response of the eastern North Atlantic subpolar gyre to the North Atlantic Oscillation, *Geophys. Res. Lett.*, 36(L17607), doi:10.1029/2009GL039090.

Holliday, N. P. (2003), Air-sea interaction and circulation changes in the northeast Atlantic, *J. Geophys. Res.*, 108(3259), doi:10.1029/2002JC001344.

Huang, B., Y. Xue, A. Kumar, and D. W. Behringer (2012), AMOC variations in 1979-2008 simulated by NCEP operational ocean data assimilation system, *Clim. Dyn.*, 38(3-4), 513–525, doi:10.1007/s00382-011-1035-z.

Huck, T., A. C. de Verdière, P. Estrade, and R. Schopp (2008), Low-frequency variations of the large-scale ocean circulation and heat transport in the North Atlantic from 1955-1998 in situ temperature and salinity data, *Geophys. Res. Lett.*, 35(L23613), doi:10.1029/2008GL035635.

Hurrell, J. W. (1995), Decadal trends in the North Atlantic Oscillation: Regional temperatures and precipitation, *Science*, 269, 676–679, doi:10.1126/science.269.5224.676.

Kieke, D., M. Rhein, L. Stramma, W. M. Smethie, J. L. Bullister, and D. A. LeBel (2007), Changes in the pool of Labrador Sea Water in the subpolar North Atlantic, *Geophys. Res. Lett.*, 34(L06605), doi:10.1029/2006GL028959.

Large, W., and S. Yeager (2004), Diurnal to decadal global forcing for ocean and sea-ice models: The datasets and flux climatologies, *Note ncar/tn*, Natl. Cent. for Atmos. Res., Boulder, Colo.

Levitus, S., T. P. Boyer, M. E. Conkright, T. O'Brien, J. Antonov, C. Stephens, L. Stathoplos, D. Johnson, and R. Gelfeld (1998), World Ocean Database 1998, *NOAA Atlas NESDIS*, 18.

Lherminier, P., H. Mercier, C. Gourcuff, M. F. Alvarez, S. Bacon, and C. Kermabon (2007), Transport across the 2002 Greenland-Portugal section and comparison with 1997, *J. Geophys. Res.*, 112(C07003), doi:10.1029/2006JC003716.

Lherminier, P., H. Mercier, T. Huck, C. Gourcuff, F. F. Perez, P. Morin, A. Sarafanov, and A. Falina (2010), The Atlantic Meridional Overturning Circulation and the Subpolar Gyre observed at the A25-OVIDE Section in June 2002 and 2004, *Deep Sea Res. I*, 57(11), 1374–1391, doi:10.1016/j.dsr.2010.07.009.

Madec, G. (2008), NEMO Ocean engine, *Tech. rep.*, Institut Pierre-Simon Laplace.

Marsh, R., B. D. Cuevas, A. C. Coward, and H. L. Bryden (2005), Thermohaline circulation at three key section in the North Atlantic over 1985-2002, *Geophys. Res. Lett.*, 32(L10604), doi:10.1029/2004GL022281.

Marshall, J., H. Johnson, and J. Goodman (2001), A study of the Interaction of the North Atlantic Oscillation with Ocean Circulation, *J. Phys. Oceanogr.*, 14(7), 1399–1421, doi:10.1175/1520-0442.

Maslowski, W., D. Marble, W. Walczowski, U. Schauer, J. L. Clement, and A. J. Semtner (2004), On climatological mass, heat and salt transports through the Barent Sea and Fram Strait from a pan-Arctic coupled ice-ocean model simulation, *J. Geophys. Res.*, 109(C03032), doi:10.1029/2001JC001039.

Molines, J. M., B. Barnier, T. Penduff, L. Brodeau, A. M. Treguier, S. Theeten, and G. Madec (2006), Definition of the interannual experiment ORCA025-G70, 1958-2004, *LEGI Report*.

Nilsen, J. E. Ø., Y. Gao, H. Drange, T. Furevik, and M. Bentsen (2003), Simulated North Atlantic-Nordic Seas water mass exchanges in an isopycnic coordinate OGCM, *Geophys. Res. Lett.*, 30(1536), doi:10.1029/2002GL016597.

Olsen, S. M., B. Hansen, D. Quadfasel, and S. Østerhus (2008), Observed and modelled stability of overflow across the Greenland-Scotland ridge, *Nature*, 455, 519–522, doi:10.1038/nature07302.

Østerhus, S., W. R. Turrell, S. Jonsson, and B. Hansen (2005), Measured volume, heat and salt fluxes from the Atlantic to the Arctic Mediterranean, *Geophys. Res. Lett.*, 32(L07603), doi:10.1029/2004GL022188.

Perez-Brunius, P., T. Rossby, and R. Watts (2004), Absolute Transport of Mass and Temperature for the North-Atlantic Current Subpolar Front System, *J. Phys. Oceanogr.*, 34(8), 1870–1883, doi:10.1175/1520-0485(2004)034 < 1870:ATOMAT > 2.0.CO;2.

Rattan, S., P. G. Myers, A.-M. Treguier, S. Theeten, A. Biastoch, and C. Böning (2010), Towards an understanding of Labrador Sea salinity drift in eddy-permitting simulations, *Ocean Modell.*, 35(1-2), 77–88, doi:10.1016/j.ocemod.2010.06.007.

Reverdin, G., P. P. Niiler, and H. Valdimarsson (2003), North Atlantic Ocean surface currents, *J. Geophys. Res.*, 108(3002), doi:10.1029/2001JC001020.

Robson, J. I. (2010), Understanding the performance of a decadal prediction system, Ph.D. thesis, University of Reading, 223 pp.

Rossby, T. (1996), The North Atlantic Current and surrounding waters: At the crossroads, *Rev. Geophys.*, 34(4), 463–481, doi:10.1029/96RG02214.

Sarafanov, A., A. Falina, H. Mercier, A. Sokov, P. Lherminier, C. Gourcuff, S. Gladyshev, F. Gaillard, and N. Daniault (2012), Mean full-depth summer circulation and transports at the northern periphery of the Atlantic Ocean in the 2000s, *J. Geophys. Res.*, 117(C01014), doi:10.1029/2011JC007572.

Schmitz, W. J. J., and M. S. McCartney (1993), On the North Atlantic Circulation, *Rev. Geophys.*, 31, 29–49, doi:10.1029/92RG02583.

Serreze, M. C., A. P. Barrett, A. G. Slater, R. A. Woodgate, K. Aagaard, R. B. Lammers, M. Steele, R. Moritz, M. Meredith, and C. M. Lee (2006), The large-scale freshwater cycle of the Arctic, *J. Geophys. Res.*, 111(C11010), doi:10.1029/2005JC003424.

Steele, M., R. Morley, and W. Ermold (2001), PHC: A global ocean hydrography with a high quality Arctic Ocean, *J. Clim.*, 14(9), 2079–2087, doi:10.1175/1520-0442(2001)014 < 2079:PAGOHW > 2.0.CO;2.

The Drakkar Group (2007), Eddy permitting ocean circulation hindcasts of past decades, *CLIVAR exchanges*, 42.

Thierry, V., E. D. Boisséson, and H. Mercier (2008), Interannual variability of the Subpolar Mode Water properties over the Reykjanes Ridge during 1990-2006, *J. Geophys. Res.*, 113(C04016), doi:10.1029/2007JC004443.

Treguier, A., C. Gourcuff, P. Lherminier, H. Mercier, B. Barnier, G. Madec, J.-M. Molines, T. Penduff, L. Czeschel, and C. Böning (2006), Internal and forced variability along a section between Greenland and Portugal in the CLIPPER Atlantic model, *Ocean Dynamics*, 56(5-6), 568–580, doi:10.1007/s10236-006-0069-y.

Treguier, A.-M., M. H. England, S. R. Rintoul, G. Madec, J. L. Sommer, and J. M. Molines (2007), Southern Ocean overturning across streamlines in an eddying simulation of the Antarctic Circumpolar Current, *Ocean Science*, 3, 491–507.

Wunsch, C., and P. Heimbach (2006), Estimated decadal changes in North Atlantic meridional overturning circulation and heat fluxes 1993-2004, *J. Phys. Oceanogr.*, 36, 2012–2024, doi:10.1175/JPO2957.1.

Yeager, S., G. Karspeck, G. Danabasoglu, J. Tribbia, and H. Teng (2012), A decadal prediction case study: Late 20th Century North Atlantic ocean heat content, *J. Clim.*, 25(15), 5173–5189, doi:10.1175/JCLI-D-11-00595.1.

Zhang, R. (2010), Latitudinal dependence of Atlantic meridional overturning circulation (AMOC) variations, *Geophys. Res. Lett.*, 37(L16703), doi:10.1029/2010GL044474.